Journal of Materials Chemistry A

Accepted Manuscript

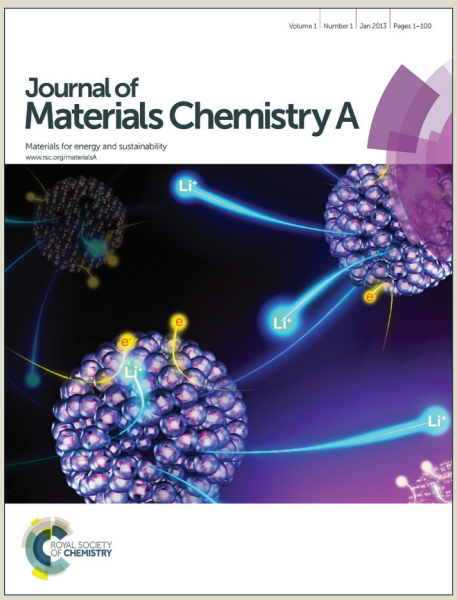

This is an *Accepted Manuscript*, which has been through the Royal Society of Chemistry peer review process and has been accepted for publication.

Accepted Manuscripts are published online shortly after acceptance, before technical editing, formatting and proof reading. Using this free service, authors can make their results available to the community, in citable form, before we publish the edited article. We will replace this *Accepted Manuscript* with the edited and formatted *Advance Article* as soon as it is available.

You can find more information about *Accepted Manuscripts* in the Information for Authors.

Please note that technical editing may introduce minor changes to the text and/or graphics, which may alter content. The journal's standard Terms & Conditions and the Ethical guidelines still apply. In no event shall the Royal Society of Chemistry be held responsible for any errors or omissions in this *Accepted Manuscript* or any consequences arising from the use of any information it contains.

ROYAL SOCIETY OF CHEMISTRY

www.rsc.org/materialsA

A general strategy for facile synthesis of AuM (M = Pt/Pd) alloyed flowerlike-assembly nanochains for enhanced oxygen reduction reaction

Li-Li He, Pei Song, Ai-Jun Wang, Jie-Ning Zheng, Li-Ping Mei, Jiu-Ju Feng*

College of Chemistry and Life Science, College of Geography and Environmental Science, Zhejiang Normal University, Jinhua, 321000, China

**Corresponding author: jjfeng@zjnu.cn (JJF), Tel./Fax: +86 579 82282269.*

Abstract

In this work, a general strategy was developed for facile synthesis of bimetallic AuM (M = Pt or Pd) alloyed flowerlike-assembly nanochains (FANs), with the assistance of diprophylline as a structure-directing agent and a stabilizing agent. The morphology, crystal structure, and compositions of AuPt and AuPd FANs were mainly investigated by transmission electron microscopy (TEM), X-ray diffraction (XRD), and X-ray photoelectron spectroscopy (XPS). The formation mechanism was discussed in some detail by varying the concentrations of diprophylline. The as-prepared AuM FANs displayed improved catalytic activity and better stability for oxygen reduction reaction (ORR) over commercial E-TEK Pt/C, Pt black and Pd black, respectively.

Keywords: Flowerlike-assembly nanochains; Bimetallic alloy; Diprophylline; Oxygen reduction reaction

Journal of Materials Chemistry A Accepted Manuscript

1. Introduction

Polymer electrolyte fuel cells (PEFCs) have attracted significant attention because of their high energy efficiency and low carbon emission.[1] The cathode electrocatalysts are critical to oxygen reduction reaction (ORR) in the overall PEFCs, because their catalytic activity and durability are strongly correlated with the cathode kinetics property.[2] As well known, platinum (Pt) and Pt nanoparticles supported on carbon material (Pt/C) are widely employed as catalysts, which are inadequate to fulfill the combined cost,[3] performance,[4] and durability requirements.[5] Also, Pd has the similar properties as compared to Pt such as the same fcc crystal structure and similar atomic size.[6]

Recently, the fabrication of bimetallic alloyed catalysts received significant attraction owing to their highly catalytic activity and better durability as contrast to single metals.[7] Researchers have prepared Pt_3Co nanocrystals,[8] PtNi nanotubes,[9] PdFe nanoparticles,[10] and AuPd nanoporous clusters,[11] which all displayed enhanced catalytic activity for ORR. Particularly, the introduction of Au into the alloyed bimetallic nanocatalysts generally brings the following advantages: enhanced catalytic activity and improved durability of the catalysts,[4] superior electrical conductivity and easier gas accessibility.

To date, AuPt and AuPd attracted increasing research interest for their intrinsic catalytic properties and good electrocatalytic performances in ORR.[12, 13] For example, AuPd alloyed nanoparticles were synthesized under hydrothermal conditions.[14] In another example, graphene-supported AuPt nanoparticles and AuPt

Journal of Materials Chemistry A Accepted Manuscript

heteronanostructures were prepared by electrodeposition method.[15, 16] Lately, graphene supported popcorn-like PtAu nanoparticles and core-shell AuPd@Pd nanocrystals were fabricated by wet-chemical method.[13]

Morphologies of bimetallic catalysts have significant influence on their catalytic activity and operation stability.[17] Many efforts have been made to construct bimetallic alloys with designed shapes,[18] especially flower-like nanostructures for their enlarged surface area, more active sites and enhanced catalytic ability.[19, 20] Meanwhile, nanochain networks also attract much attention because of their improved electrical conductivity and structural stability, which is benefit to their catalytic performance.[21] For instance, AuPd nanochain networks were prepared, which revealed improved catalytic activity towards ORR and methanol oxidation reaction as compared to commercial Pt catalyst (E-TEK).[22] Combining the advantages of nanoflowers and nanochains networks, flowerlike-assembly nanochains (FANs) might possess superior catalytic performance.

Herein, a group of AuM (M = Pt or Pd) alloyed FANs were prepared by a simple and facile one-pot strategy, using diprophylline as a structure-directing agent, without any seed, template, or surfactant. The catalytic performance of the as-prepared hybrid nanocrystals was examined using ORR as a model system.

2. Experimental section

2.1 Chemicals

Chloroplatinic acid (H_2PtCl_6), chlorauric acid ($HAuCl_4$), palladium chloride

Journal of Materials Chemistry A Accepted Manuscript

($PdCl_2$), diprophylline, hydrazine hydrate ($N_2H_4 \cdot H_2O$), commercial E-TEK Pt/C, Pt black and Pd black were purchased from Shanghai Aladdin Chemical Reagent Company (Shanghai, China). Other chemicals were of analytical grade and used without further purification. For preparation of H_2PdCl_4 solution (100 mM), 1.77 g $PdCl_2$ was dissolved into 0.4 mL HCl (37%), and then diluted to 100 mL with water. All the aqueous solutions were prepared with twice-distilled water throughout the whole experiment.

2.2 Synthesis of AuPt FANs and AuPd FANs

For typical synthesis of AuPt FANs, 100 μL of $HAuCl_4$ (24.28 mM) and 62.92 μL of H_2PtCl_6 (38.62 mM) were simultaneously put into 10 mL diprophylline solution (10 mM) in an ice bath with vigorous stirring. Then, 100 μL of hydrazine hydrate was quickly dropped into the mixed solution. The mixture quickly turned black and further reacted for 10 min. The final products were collected by centrifugation, and washed thoroughly with water for further characterization. Similarly, AuPd FANs was prepared using 100 μL of $HAuCl_4$ (24.28 mM) and 24.3 μL of H_2PdCl_4 (100 mM) as precursors, while other conditions were kept the same.

2.3 Characterization

The detailed morphology, crystal structure, and composition of the samples were determined by transmission electron microscopy (TEM), high-resolution TEM (HRTEM), high-angle annular dark-field scanning transmission electron microscopy

Journal of Materials Chemistry A Accepted Manuscript

(HAADF-STEM), and energy-dispersive X-ray spectroscopy (EDS) on a JEM-2100F microscope operated at an acceleration voltage of 200 kV. X-ray photoelectron spectroscopy (XPS) measurements were performed with a Thermo VG ESCALAB 250 spectrometer with an Al Kα X-ray radiation (1486.6 eV photons) for excitation operated at 120 W. X-ray diffraction (XRD) spectra were recorded on a Philips PW3040/60 diffractometer using Cu Kα radiation source (λ = 0.15405 nm). The specific surface area of the sample was measured by Brunauer-Emmett-Teller (BET) method on a Surface Area Analyzer (NOVA2000-09, USA) at 77.3 K through N_2 adsorption. The sample was dried at 90 °C for 4 h and then degassed at 300 °C for 1 h before determination. The morphological evolution of AuPt and AuPd FANs was determined by TEM measurements. The samples were collected from glassy carbon rotating disk electrode by ultrasonication and then dissolved in twice-distilled water uniformly before characterization.

2.4 Electrochemical measurements

The electrochemical measurements were conducted on a CHI832b electrochemical workstation (CH Instruments, Chenhua Co., Shanghai, China). Conventionally, a three-electrode system was employed for all electrochemical experiments, which consisted of a platinum wire as the auxiliary electrode, a saturated calomel reference electrode (SCE) as the reference electrode, and a bare, modified glassy carbon electrode (GCE, 3 mm in diameter), or glassy carbon rotating disk electrode (GCRDE, 4 mm in diameter) as the working electrode. Rotating disk

Journal of Materials Chemistry A Accepted Manuscript

electrode measurements were carried out on the Gamry's Rotating Disk Electrode (RDE 710). All the potentials were referred to reversible hydrogen electrode (RHE) in this work.

For typical preparation of AuPt FANs modified electrodes, 5 mg of the sample was put into 5 mL of water under ultrasonication for 30 min to obtain a homogeneous suspension (1 mg mL^{-1}). Then, 6 and 15 μL of the suspensions were dropped onto the surfaces of the clean GCE and GCRDE, and dried in air naturally, followed by covering another layer of Nafion (0.05 wt%) with the volumes of 4 and 6 μL, respectively. Meanwhile, AuPd FANs, commercial E-TEK Pt/C, Pt black and Pd black modified electrodes were prepared in the same way. The metal loadings are 0.085 and 0.120 mg cm^{-2} for these catalyst-modified GCE and GCRDE, respectively.

CO-stripping measurements on the catalyst modified electrodes were performed as follows: CO was bubbled for 30 min to form CO ad-layer on the catalyst surface at a fixed potential of 0.142 V (*vs.* RHE). Excess CO in the electrolyte was purged with N_2 for 30 min and CO-stripping voltammograms were acquired via the oxidation of the pre-adsorbed CO in 0.5 M H_2SO_4 at the scan rate of 50 mV s^{-1}. The electrochemically active surface area (ECSA) of the catalyst was calculated by the following equation: [23]

$$\text{ECSA} = \frac{Q}{C \times m} \quad (1)$$

where Q is the charge for CO desorption-electrooxidation, m represents the amount of Pt and Pd on the electrode surface (mg), and C (210 or 420 μC cm^{-2}) is the charge needed to oxidize a monolayer of CO on Pt or Pd catalysts, respectively.

Journal of Materials Chemistry A Accepted Manuscript

The ORR polarization curves were obtained in O_2-saturated 0.1 M KOH with a sweep rate of 5 mV s^{-1} at various rotating speeds ranging from 100 to 2500 rpm. The Koutecky-Levich plots (obtained by using the inverse current density (j^{-1}) as a function of the inverse of the square root of the rotating rate ($\omega^{-1/2}$)) were analyzed at 0.61 V (*vs.* RHE). The slopes of the linear fitting lines are used to calculate the number of transferred electrons (n) according to the following Koutecky-Levich equation:

$$\frac{1}{i} = \frac{1}{i_k} + \frac{1}{i_d} = \frac{1}{i_k} + \frac{1}{B\omega^{1/2}} \quad (2)$$

$$B = 0.2nFC_0D_0^{2/3}v^{-1/6} \quad (3)$$

where i_k is the kinetic current, i_d is the diffusion-limiting current, i is the measured current, ω is the rotating speed, n is the number of the transferred electrons, F is the Faraday constant (96485 C mol^{-1}), C_0 is the oxygen solubility (1.2×10^{-3} mol L^{-1}), D_0 is the oxygen diffusivity (1.9×10^{-5} cm^2 s^{-1}), and v is the kinetic viscosity of the electrolyte (0.01 cm^2 s^{-1}).[24] By putting these parameters into the equation (3), namely, $B = 0.0376\,n$, B factor can be calculated from the respective slopes.

3. Results and discussion

Low- and middle-magnification TEM images (Fig. 1A, B and Fig. 2A, B) show that the typical products contain a lot of well-dispersed nanochains assembled by many nanoflowers with a length of several micrometers, as strongly supported by the FESEM images (Fig. S1, Electronic Supplementary Information, ESI). Furthermore, HRTEM images are recorded at the marked junctions of AuPt (Fig. 1C and D) and

Journal of Materials Chemistry A Accepted Manuscript

AuPd (Fig. 2C and D) FANs. The well-defined lattice fringes confirm that the respective junctions are fused together by crystal growth. The corresponding d-spacing values are determined from the marked regions, with the values of 0.232 and 0.230 nm for AuPt and AuPd FANs, respectively, corresponding to the (111) planes of the face centered cubic (fcc) AuPt and AuPd alloys.[25, 26] Furthermore, the associated SAED patterns (insets in Fig. 1A and Fig. 2A) strongly manifest their polycrystalline nature. Additionally, based on the EDS measurements, the Au/Pt and Au/Pd atomic ratios in AuPt and AuPd FANs are 1/1.02 and 1/1.26, which are approximate to the stoichiometric proportion of the initial precursors.

HRTEM images show the interconnected porous structures of AuPt (Fig. 1C, D) and AuPd (Fig. 2C, D) FANs. Their porous properties are further demonstrated by the data from N_2 adsorption-desorption isotherms determination (Fig. S2, ESI). The hysteresis loops are associated with narrow slit-like pores in the samples. The BET specific surface areas are calculated to be 13.44 $m^2 g^{-1}$ for AuPt FANs and 10.65 $m^2 g^{-1}$ for AuPd FANs (Table S1, ESI). Besides, there are two peaks observed for the corresponding pore size-distribution curves, respectively. And the average pore diameters are 24.76 nm and 26.43 nm for agglomerated AuPt and AuPd FANs, respectively, with the pore sizes of 1.75 nm for AuPt FANs and 1.67 nm for AuPd FANs.

For comparison, the morphology features of the commercial Pt/C, Pt black and Pd black are also elucidated by TEM analysis (Fig. S3A-C, ESI). Notably, there are many well-dispersed spherical nanoparticles, with their average sizes of around 4.25

Journal of Materials Chemistry A Accepted Manuscript

nm, 4.63 and 18.55 nm obtained from their histograms for commercial Pt/C (inset in Fig. S3A), Pt black (inset in Fig. S3B), and Pd black (inset in Fig. S3 C), respectively.

Fig. 1F depicts the XRD pattern of AuPt FANs. Specifically, there are four representative diffraction peaks emerged at 38.81°, 45.02°, 66.41°, and 79.01°, which are matched well with the (111), (200), (220), and (311) planes of the fcc AuPt alloy.[27] These peaks are coincidently located between bulk Au (JCPDS-04-0784) and Pt (JCPDS-04-0802), further showing the alloyed feature of AuPt FANs. Similarly, the XRD pattern of AuPd FANs also indicates their alloyed feature (Fig. 2F).

More importantly, the particle size of AuM FANs can be calculated from the line broadening of the (111) diffraction peak according to Scherrer's equation, $L = (0.9\ \lambda) / (\beta_{1/2}\ cos\theta)$, where λ is the wavelength of the X-ray (1.5406 Å), θ is the angle at the position of the peak maximum, and $\beta_{1/2}$ is the width of the diffraction peak at half height in radians.[13] According to the calculation, the particle sizes are 3.1 nm for AuPt FANs, 7.2 nm for Pt black, 5.1 nm for AuPd FANs, and 18.2 nm for Pd black, respectively.

HAADF-STEM elemental mapping images (Fig. 3A and 4A) show that Au atoms are homogeneously dispersed on the surface of AuM FANs. Besides, the line scanning curve of Au is completely overlapped with that of Pt/Pd throughout the whole AuM FANs (Fig. 3B and 4B), revealing similar amounts of Au atoms to those of Pt/Pd, along with the coexistence of Au and Pt/Pd on the surface of AuPt (or AuPd) FANs, reflecting the alloy feature of AuPt (or AuPd).

XPS is a useful tool to analyze the valence states and surface composition of

Journal of Materials Chemistry A Accepted Manuscript

nanomaterials. Fig. 5 displays high-resolution XPS spectra of Au 4f (A) and Pt 4f (B) for AuPt FANs, and Au 4f (C) and Pd 3d (D) for AuPd FANs, respectively. The distinct peaks confirm the coexistence of these elements in the as-prepared nanochains, which can be divided into two pairs of Lorentzian curves, respectively. The stronger pair is assigned to Au^0 or M^0 (M = Pt, Pd), while the weaker couple corresponds to Au^{3+} or M^{n+}. From their peak intensities, we can conclude that metallic Au^0 and M^0 are the predominant species. Moreover, the respective atomic ratios of Au/Pt and Au/Pd on the FANs surfaces are 1.12 and 1.17, respectively. These values are much close to those obtained from the EDS data, further confirming the formation of AuM alloys. Table S2 in ESI provides the associated binding energies of each composition in AuM alloys. Moreover, no peak of N element is observed in the XPS survey spectrum (Fig. S4, ESI), which indicates that diprophylline is easily removed from the materials surface.

The formation mechanism of the as-prepared nanochains is discussed, using AuPt FANs as an example. Initially, when $HAuCl_4$ and H_2PtCl_6 are put into the aqueous diprophylline solution under stirring, diprophylline-$AuCl_4^-$/$PtCl_6^{2-}$ complexes are formed. Upon the addition of hydrazine hydrate, a large numbers of Au and Pt atoms are quickly produced at the very early stage,[28] which is quickly stabilized by the released diprophylline molecules. Moreover, as confirmed by the previous reports, the dipole-dipole attraction leads to the formation of nanochains.[14, 29] It is known that different crystal planes possess different surface energy, which would cause selective adsorption of diprophylline on specific crystal planes.[29] Then, the “bare” surfaces can

Journal of Materials Chemistry A Accepted Manuscript

orient to each other because of the hydrophobic effects, while the "covered" ones can repel each other and stabilize in the present system. Thus, a delicate equilibrium between the attraction and repulsion is responsible for the formation of AuPt FANs.

As expected, the amount of diprophylline is essential to the morphology of the product. Specifically, the absence of diprophylline yields heavily aggregated AuPt nanoparticles (Fig. 6A). Stochastic collisions usually occur between the adjacent nanoparticles if they are uncovered by diprophylline. As a result, aggregated nanoparticles are formed via repeating the adhesion of nanoparticles. Increasing the concentration of diprophylline from 2 (Fig. 6B) to 10 mM (Fig. 1A) produces nanochains with increased length that are assembled by flower-like nanoparticles. More diprophylline can strengthen dipole-dipole attractions, which benefits to extend the length of nanochains. Conversely, excess diprophylline such as 25 (Fig. 6C) and 50 mM (Fig. 6D) induce the formation of shortened nanochains or even nanoflowers. In this case, the surfaces of AuPt nanoparticles are fully covered with diprophylline to enhance their stability in the solution and even keep them from linking together,[30] leading to the emergence of shortened nanochains and even single nanoflowers, respectively. Similar trends are observed for AuPd products (Fig. 7), except the formation of mild aggregated nanoparticles with 2.5 mM diprophylline (Fig. 7B).

Linear sweep voltammetry and cyclic voltammetry experiments were employed to investigate the electrocatalytic performance of AuPt and AuPd FANs modified electrodes, using commercial Pt black and Pd black as referenced materials. For better comparison, all the electrochemical data were normalized by the geometrical surface

Journal of Materials Chemistry A Accepted Manuscript

area of the electrode (i.e., 0.07065 cm^{-2} for glassy carbon electrode, 0.1256 cm^{-2} for rotating disk electrode). Fig. 8A and B show the corresponding cyclic voltammetry (CV) curves of the catalysts modified electrodes. These catalysts modified electrodes display well-defined hydrogen desorption/adsorption and metal oxidation/reduction peaks. Specifically, in the forward scan, hydrogen desorption peaks appear at 0.042 ~ 0.342 V (*vs.* RHE), and hydroxyl species (OH_{ad}) adsorption peaks emerge beyond 0.842 V (*vs.* RHE). In the backward sweep, the OH_{ad} reduction peaks come out at 0.642 ~ 0.842 V (*vs.* RHE), and hydrogen is adsorbed below 0.342 V (*vs.* RHE). The onset potentials for OH_{ad} desorption positively shift for AuPt and AuPd FANs modified electrodes compared with the other catalysts modified electrodes, suggesting weak affinity of OH_{ad} on the surfaces of AuM FANs, which is benefit to ORR.[13, 31]

The ECSA is closely associated with the number of available active sites,[32] which is calculated from CO-stripping voltammograms. The ECSA is 39.01 $m^2 g^{-1}$ for AuPt FANs (Fig. 9A), which is larger than that of commercial Pt black (18.56 $m^2 g^{-1}$, Fig. 9B). Besides, the ECSA (34.50 $m^2 g^{-1}$, Fig. 9C) is also larger for AuPd FANs than those of commercial Pd black (14.60 $m^2 g^{-1}$, Fig. 9D) and E-TEK Pt/C (7.85 $m^2 g^{-1}$, Fig. S5, ESI).

Liu et al. demonstrated that the electrochemical surface areas are closely related to the particle sizes of the catalysts, which is in agreement with the trend that catalyst nanoparticles with smaller sizes have larger ECSA values.[31, 33] In our work, the particle sizes are 3.1 nm for AuPt FANs and 5.1 nm for AuPd FANs, respectively. These values are smaller than Pt black (7.2 nm) and Pd black (18.2 nm). Therefore,

Journal of Materials Chemistry A Accepted Manuscript

the particle sizes of AuM FANs contribute to the larger ECSAs. Additionally, many pores are existed in the nanoflowers, which are also responsible for the enlarged ECSA.[34]

Fig. 10A and C display the ORR polarization curves of AuPt FANs, AuPd FANs, commercial E-TEK Pt/C, Pt black, and Pd black modified electrodes in O_2-saturated 0.1 M KOH at a scan rate of 5 mV s^{-1} with a rotating rate of 1600 rpm. Clearly, the onset potential (0.932 V *vs.* RHE) is more positive for AuPt FANs, compared with those of commercial Pt black (0.922 V *vs.* RHE) and E-TEK Pt/C (0.886 V *vs.* RHE). Besides, the half-wave potential is 0.870 V (*vs.* RHE) for AuPt FANs, which is more positive than those of commercial Pt black (0.830 V *vs.* RHE) and E-TEK Pt/C (0.771 V *vs.* RHE). Similar trend is obtained in the case of AuPd FANs under the identical conditions. These results reveal the improved catalytic activity of AuPt and AuPd FANs in the present system.

It is known that the kinetic current density (i_k) represents the intrinsic catalytic activity. The specific and mass kinetic activities are obtained by normalizing the kinetic current densities to the ECSA and mass of these catalysts. As revealed in Fig. 10B, the specific activity is 0.55 mA cm^{-2} at 0.71 V (*vs.* RHE) for AuPt FANs, which is 2.50 and 1.06 times larger than those of commercial Pt black (0.22 mA cm^{-2}) and E-TEK Pt/C (0.52 mA cm^{-2}). Besides, the mass activity of AuPt FANs is 215.24 mA mg^{-1}, which is nearly 5.26 and 1.19 times higher than those of commercial Pt black (40.91 mA mg^{-1}) and E-TEK Pt/C (180.40 mA mg^{-1}). Similarly, the specific and mass activities are 0.56 mA cm^{-2} and 193.73 mA mg^{-1} for AuPd FANs at 0.71 V (*vs.* RHE),

Journal of Materials Chemistry A Accepted Manuscript

respectively, which are larger than those for commercial Pd black (0.35 mA cm^{-2}, 51.69 mA mg^{-1}) and E-TEK Pt/C (0.52 mA cm^{-2}, 180.40 mA mg^{-1}). Furthermore, these values are larger than those of Pt nanochain networks (0.27 mA cm^{-2}, 37 mA mg^{-1}),[35] Pt-Pd-Co trimetallic alloyed network (45 mA mg^{-1})[31] and core-shell AuPd@Pd nanocrystals (0.40 mA cm^{-2}, 174 mA mg^{-1}).[36] Compared with the similar work that our group had reported previously (Table S3, ESI), the mass activity of AuM FANs larger than Pt_3Co[37] and PtPd[38] nanoflower. In addition, the AuM FANs possess higher values than that of PtAu-rGO[13] in term of the special activity.

Randomly choosing another applied potential of 0.9 V, the mass and specific activities of AuPt FANs are estimated to be 155.34 mA mg^{-1} and 0.43 mA cm^{-2}, which are roughly 4.35 and 1.32 times higher than those of commercial Pt black (35.71 mA mg^{-1}, 0.17 mA cm^{-2}). Similarly, the mass and specific activities of AuPd FANs are 142.21 mA mg^{-1} and 0.48 mA cm^{-2}, which are larger than those for commercial Pd black (34.87 mA mg^{-1}, 0.24 mA cm^{-2}) under the same conditions. There results demonstrate the improved performances of AuM in comparison with the referenced catalysts.

To evaluate the transferred electron number (n) of AuPt FANs, the corresponding ORR polarization curves were recorded in O_2-saturated 0.1 M KOH at a scan rate of 5 mV s^{-1} with different rotating rates (Fig. 11A-C), using commercial Pt black and E-TEK Pt/C as standards. Similarly, the ORR polarization curves of AuPd FANs, commercial Pd black, and E-TEK Pt/C modified electrodes were obtained under the same conditions (Fig. 12A-C). According to the Koutecky-Levich plots (Fig.

Journal of Materials Chemistry A Accepted Manuscript

11C and Fig. 12C), the *n* values are calculated to be 4.15, 4.01, 4.05, 4.06, and 4.03 at 0.71 V (*vs.* RHE) for AuPt FANs, AuPd FANs, commercial Pt black, Pd black, and E-TEK Pt/C, respectively, indicating the efficient reduction of O_2 to H_2O via a direct four-electron pathway.[39, 40] The *n* values are slight above 4.0, possibly owing to the inhomogeneous coverage of the catalyst on the electrode surface during the fabrication procedure. As a result, the whole currents are not only come from the kinetic currents (i_d), and also the diffusion-limiting currents (i_k) involved via the bare electrode surface.

The durability of a catalyst is an important issue to be considered before its commercial application in fuel cells.[1, 41] Therefore, the accelerated stability test was conducted by applying continuous potential sweeps between 0.21 and 1.21 V (*vs.* RHE) in O_2-saturated 0.1 M KOH at a scan rate of 5 mV s^{-1}. After 1000 cycles, the half-wave potentials only negatively shift about 4 and 7 mV for AuPt (Fig. 13A) and AuPd (Fig. 13C) FANs, respectively, while there are 13 mV, 11 mV, and 71mV negative shifts in the cases of commercial Pt black (Fig. 13B), Pd black (Fig. 13D) and E-TEK Pt/C (Fig. S6, ESI). These results indicate the improved stability of AuM FANs.

After the durability test, the morphological evolution of AuPt and AuPd FANs was examined by TEM measurements to further evaluate their stability (Fig. S7, ESI). Clearly, the structures of FANs are still remained, and no obvious agglomeration/dissolution was observed for AuPt and AuPd FANs, reflecting the improved durability of AuPt and AuPd FANs. This is due to the unique interconnected

Journal of Materials Chemistry A Accepted Manuscript

structures of AuPt and AuPd FANs which can suppress the Ostwald ripening, as confirmed by the literature.[33, 42]

The enhanced performances of AuPt and AuPd FANs are mainly ascribed to the interconnected porous bimetallic alloyed structures, which provide the enlarged ECSAs and more active sites available for ORR, promote O_2 diffusion and electron transport,[43] and suppress the Ostwald ripening.[44] Furthermore, the highly ordered structures and tight interconnection of AuM FANs facilitate the mass transportation of reactant molecules, increase the electrochemically utilized Pt/Pd atoms, and enhance the ORR activity.[45, 46]

More importantly, the synergistic effects of Au and M (Pt or Pd) herein play important roles. Evidently, the modified electronic structures of Pt/Pd with Au can facilitate the breaking of Pt-OH_{ad} or Pd-OH_{ad}, which are beneficial to inhibiting the formation of Pt-OH_{ad} and Pd-OH_{ad}. Accordingly, the concentration of Pt-OH_{ad} or Pd-OH_{ad} on the surface of AuM FANs is significantly reduced in comparison with that on commercial Pt/Pd black. This characteristic improves the kinetics and efficiently enhance the ORR catalytic activity, as evidenced by the positive shifts of the OH_{ad} desorption potentials in CV curves (Fig. 8). This assumption is supported by the density functional theory study of the electronic interactions between Pt/Pd and its substrate,[47] owing to the decreased Gibbs free energy of electron transfer by alloying.[48] In addition, the "clean" surface of AuM FANs promotes the catalytic performance of ORR,[49] because diprophylline is easily removed from AuM FANs surfaces as compared to surfactant or polymers.[50]

Journal of Materials Chemistry A Accepted Manuscript

4. Conclusion

In summary, a facile and rapid one-pot method was developed for synthesis of AuPt and AuPd FANs, while no seed, surfactant, or template involved. The as-prepared AuPt and AuPd nanocrystals offer the enlarged ECSAs and efficient electron transport path, resulting in the enhanced electrocatalytic activity and better stability for ORR in alkaline media, compared with commercial Pt black, Pd black, and E-TEK Pt/C. The superior catalytic properties are ascribed to the synergetic effects between Pt and Au in AuPt FANs, Pd and Au in AuPd FANs, as well as their unique interconnected porous nanostructures. The synthesis strategy would provide a promising method for fabrication of novel Au-based catalysts in fuel cells.

Acknowledgements

This work was financially supported by National Natural Science Foundation of China (Nos. 21475118, 21175118 and 21275130), and Zhejiang province university young academic leaders of academic climbing project (No. pd2013055).

References

1. K. Sasaki, H. Naohara, Y. Cai, Y. M. Choi, P. Liu, M. B. Vukmirovic, J. X. Wang and R. R. Adzic, Adzic, *Angew. Chem.*, 2010, **49**, 8602-8607.
2. B. Lim, M. Jiang, P. H. C. Camargo, E. C. Cho, J. Tao, X. Lu, Y. Zhu and Y. Xia, Science, 2009, **324**, 1302-1305.

Journal of Materials Chemistry A Accepted Manuscript

3. H.-W. Liang, W. Wei, Z.-S. Wu, X. Feng and K. Müllen, *J. Amer. Chem. Soc.*, 2013, **135**, 16002-16005.

4. A. Tewari, V. Sambhy, M. Urquidi Macdonald and A. Sen, *J. Power Sources*, 2006, **153**, 1-10.

5. S. Ghosh, R. K. Sahu and C. R. Raj, *J. Mater. Chem.*, 2011, **21**, 11973-11980.

6. E. Antolini, *Energy Environ. Sci*, 2009, **2**, 915-931.

7. B. Wang, *J. Power Sources*, 2005, **152**, 1-15.

8. S.-I. Choi, R. Choi, S. W. Han and J. T. Park, *Chem. Eur. J.*, 2011, **17**, 12280-12284.

9. S. Du, Y. Lu, S. K. Malladi, Q. Xu and R. Steinberger-Wilckens, *J. Mater. Chem. A*, 2014, **2**, 692-698.

10. M.-H. Shao, K. Sasaki and R. R. Adzic, *J. Amer. Chem. Soc.*, 2006, **128**, 3526-3527.

11. Y. Li, E. Zhu, Y. Chen, C. Chiu, H. Yu, X. Huang, R. Hicks and Y. Huang, *ChemSusChem*, 2013, **6**, 1868-1872.

12. D. I. Enache, J. K. Edwards, P. Landon, B. Solsona-Espriu, A. F. Carley, A. A. Herzing, M. Watanabe, C. J. Kiely, D. W. Knight and G. J. Hutchings, *Science*, 2006, **311**, 362-365.

13. J.-N. Zheng, S.-S. Li, X. Ma, F.-Y. Chen, A.-J. Wang, J.-R. Chen and J.-J. Feng, *J. Mater. Chem. A*, 2014, **2**, 8386-8395.

14. J. H. Shim, J. Kim, C. Lee and Y. Lee, *Chem. Mater.*, 2011, **23**, 4694-4700.

15. Y. Hu, H. Zhang, P. Wu, H. Zhang, B. Zhou and C. Cai, *Phys. Chem. Chem. Phys.*,

Journal of Materials Chemistry A Accepted Manuscript

2011, **13**, 4083-4094.

16. Y. Kim, J. W. Hong, Y. W. Lee, M. Kim, D. Kim, W. S. Yun and S. W. Han, *Angew. Chem.*, 2010, **122**, 10395-10399.

17. J. W. Hong, D. Kim, Y. W. Lee, M. Kim, S. W. Kang and S. W. Han, *Angew. Chem. Int. Ed.*, 2011, **50**, 8876-8880.

18. J. Chen, B. Lim, E. P. Lee and Y. Xia, *Nano Today*, 2009, **4**, 81-95.

19. J. Xu, A. R. Wilson, A. R. Rathmell, J. Howe, M. Chi and B. J. Wiley, *ACS Nano*, 2011, **5**, 6119-6127.

20. G. Fu, K. Wu, J. Lin, Y. Tang, Y. Chen, Y. Zhou and T. Lu, *J. Phys. Chem. C*, 2013, **117**, 9826-9834.

21. C. Xu, L. Wang, R. Wang, K. Wang, Y. Zhang, F. Tian and Y. Ding, *Adv. Mater.*, 2009, **21**, 2165-2169.

22. A. Cha, J. H. Shim, A. Jo, S. C. Lee, Y. Lee and C. Lee, *Electroanal*,, 2014, **26**, 723-731.

23. S.-S. Li, J.-J. Lv, Y.-Y. Hu, J.-N. Zheng, J.-R. Chen, A.-J. Wang and J.-J. Feng, *J. Power Sources*, 2014, **247**, 213-218.

24. L. Tammeveski, H. Erikson, A. Sarapuu, J. Kozlova, P. Ritslaid, V. Sammelselg and K. Tammeveski, *Electrochem. Commun.*, 2012, **20**, 15-18.

25. X. Cao, N. Wang, S. Jia, L. Guo and K. Li, *Biosens. Bioelectron.*, 2013, **39**, 226-230.

26. J. W. Hong, Y. W. Lee, M. Kim, S. W. Kang and S. W. Han, *Chem. Commun.*, 2011, **47**, 2553-2555.

Journal of Materials Chemistry A Accepted Manuscript

27. J. Xu, T. Zhao, Z. Liang and L. Zhu, *Chem. Mater.*, 2008, **2**0, 1688-1690.

28. F. Wang, C. Li, L.-D. Sun, C.-H. Xu, J. Wang, J. C. Yu and C.-H. Yan, *Angew. Chem. Int. Ed.*, 2012, **51**, 4872-4876.

29. J. R. Windmiller, N. Zhou, M.-C. Chuang, G. Valdes-Ramirez, P. Santhosh, P. R. Miller, R. Narayan and J. Wang, *Analyst*, 2011, **136**, 1846-1851.

30. A. Zilman, T. Tlusty and S. A. Safran, *J. Phys.: Condens. Matter*, 2003, **15**, S57-S64.

31. X. Liu, G. Fu, Y. Chen, Y. Tang, P. She and T. Lu, *Chem. Eur. J.*, 2014, **20**, 585-590.

32. J.-N. Zheng, J.-J. Lv, S.-S. Li, M.-W. Xue, A.-J. Wang and J.-J. Feng, *J. Mater. Chem. A*, 2014, **2**, 3445-3451.

33. J. Xu, X. Liu, Y. Chen, Y. Zhou, T. Lu and Y. Tang, *J. Mater. Chem.*, 2012, **22**, 23659-23667.

34. X. Chen, Z. Cai, X. Chen and M. Oyama, *J. Mater. Chem. A*, 2014, **2**, 315-320.

35. J. Xu, G. Fu, Y. Tang, Y. Zhou, Y. Chen and T. Lu, *J. Mater. Chem.*, 2012, **22**, 13585-13590.

36. J.-N. Zheng, S.-S. Li, X. Ma, F.-Y. Chen, A.-J. Wang, J.-R. Chen and J.-J. Feng, *J. Power Sources*, 2014, **262**, 270-278.

37. J.-N. Zheng, L.-L. He, C. Chen, A.-J. Wang, K.-F. Ma and J.-J. Feng, *J. Power Sources*, 2014, **268**, 744-751.

38. J.-N. Zheng, L.-L. He, F.-Y. Chen, A.-J. Wang, M.-W. Xue and J.-J. Feng, *Electrochim. Acta*, 2014, **137**, 431-438.

Journal of Materials Chemistry A Accepted Manuscript

39. J.-J. Lv, J.-X. Feng, S.-S. Li, Y.-Y. Wang, A.-J. Wang, Q.-L. Zhang, J.-R. Chen and J.-J. Feng, *Electrochim. Acta*, 2014, **133**, 407-413.

40. X.-R. Li, X.-L. Li, M.-C. Xu, J.-J. Xu and H.-Y. Chen, *J. Mater. Chem. A*, 2014, **2**, 1697-1703.

41. H.-W. Liang, X. Cao, F. Zhou, C.-H. Cui, W.-J. Zhang and S.-H. Yu, *Adv. Mater.*, 2011, **23**, 1467-1471.

42. S. Sun, G. Zhang, D. Geng, Y. Chen, R. Li, M. Cai and X. Sun, *Angew. Chem*, 2011, **123**, 442-446.

43. Y. Qiao and C. M. Li, *J. Mater. Chem.*, 2011, **21**, 4027-4036.

44. J. H. Shim, Y. S. Kim, M. Kang, C. Lee and Y. Lee, *Phys. Chem. Chem. Phys.*, 2012, **14**, 3974-3979.

45. S. H. Joo, S. J. Choi, I. Oh, J. Kwak, Z. Liu, O. Terasaki and R. Ryoo, *Nature*, 2001, **412**, 169-172.

46. S. Song, Y. Liang, Z. Li, Y. Wang, R. Fu, D. Wu and P. Tsiakaras, *Appl. Catal. B Environ.*, 2010, **98**, 132-137.

47.J. Zhang, M. B. Vukmirovic, Y. Xu, M. Mavrikakis and R. R. Adzic, *Angew. Chem. Int. Ed.*, 2005, **44**, 2132-2135.

48. Y. Wang and P. B. Balbuena, *J. Phys. Chem. B*, 2005, **109**, 18902-18906.

49. X. Chen, G. Wu, J. Chen, X. Chen, Z. Xie and X. Wang, *J. Am. Chem. Soc.*, 2011, **133**, 3693-3695.

50. L. L. He, J. N. Zheng, J. J. Feng, P. Song, S.-X. Zhong, A. J. Wang and Z. Chen, *J.Power Sources*, 2014, **276**, 357-364.

Journal of Materials Chemistry A Accepted Manuscript

Captions

Fig. 1 (A, B) TEM and (C, D) HRTEM images of AuPt FANs. The corresponding (E) EDS and (F) XRD patterns. Inset shows the corresponding SAED pattern.

Fig. 2 (A, B) TEM and (C, D) HRTEM images of AuPd FANs. The corresponding (E) EDS and (F) XRD patterns. Inset shows the corresponding SAED pattern.

Fig. 3 (A) HAADF-STEM-EDS mapping images of AuPt FANs. (B) The corresponding HAADF-STEM image and cross-sectional compositional line profiles.

Fig. 4 (A) HAADF-STEM-EDS mapping images of AuPd FANs. (B) The corresponding HAADF-STEM image and cross-sectional compositional line profiles.

Fig. 5 High-resolution XPS spectra of (A) Au 4f and (B) Pt 4f in AuPt FANs, and (C) Au 4f and (D) Pd 3d in AuPd FANs.

Fig. 6 TEM images of AuPt FANs obtained with different concentrations of diprophylline: (A) 0 mM, (B) 2.5 mM, (C) 25 mM, and (D) 50 mM.

Fig. 7 TEM images of AuPd FANs obtained in the presence of different concentrations of diprophylline: (A) 0 mM, (B) 2 mM, (C) 25 mM, and (D) 50 mM.

Journal of Materials Chemistry A Accepted Manuscript

Fig. 8 CV curves of (A) AuPt FANs (curve a) and commercial Pt black (curve b), (B) AuPd FANs (curve a) and commercial Pd black (curve b) modified electrodes in N_2-saturated 0.5 M H_2SO_4 at a scan rate of 50 mV s^{-1}.

Fig. 9 CO-stripping voltammograms of (A) AuPt FANs, (B) commercial Pt black, (C) AuPd FANs, and (D) commercial Pd black modified electrodes in 0.5 M H_2SO_4 at a scan rate of 50 mV s^{-1}.

Fig. 10 ORR polarization curves of (A) AuPt FANs (curve a), Pt black (curve b) and commercial E-TEK Pt/C (curve c), (C) AuPd FANs (curve a), commercial Pd black (curve b) and E-TEK Pt/C (curve c) modified electrodes in O_2-saturated 0.1 M KOH at the rotating rate of 1600 rpm using a scan rate of 5 mV s^{-1}. (B, D) The corresponding specific and mass activities given as kinetic current densities normalized against the ECSA and mass of these catalysts, respectively.

Fig. 11 Polarization curves of ORR on (A) AuPt FANs, (B) commercial Pt black and (C) E-TEK Pt/C modified electrodes in O_2-saturated 0.1 M KOH at different rotating rates at the scan rate of 5 mV s^{-1}. (D) The corresponding Koutecky-Levich plots at 0.61 V *vs.* RHE.

Fig. 12 Polarization curves of ORR on (A) AuPd FANs, (B) commercial Pd black and (C) E-TEK Pt/C modified electrodes in O_2-saturated 0.1 M KOH at different rotating

Journal of Materials Chemistry A Accepted Manuscript

rates with a scan rate of 5 mV s^{-1}. (D) The corresponding Koutecky-Levich plots at 0.61 V *vs.* RHE.

Fig. 13 ORR polarization curves of (A) AuPt FANs, (B) commercial Pt black, (C) AuPd FANs, and (D) commercial Pd black modified electrodes before and after 1000 potential cycles at a scan rate of 5 mV s^{-1}.

Journal of Materials Chemistry A Accepted Manuscript

Figures

Fig. 1

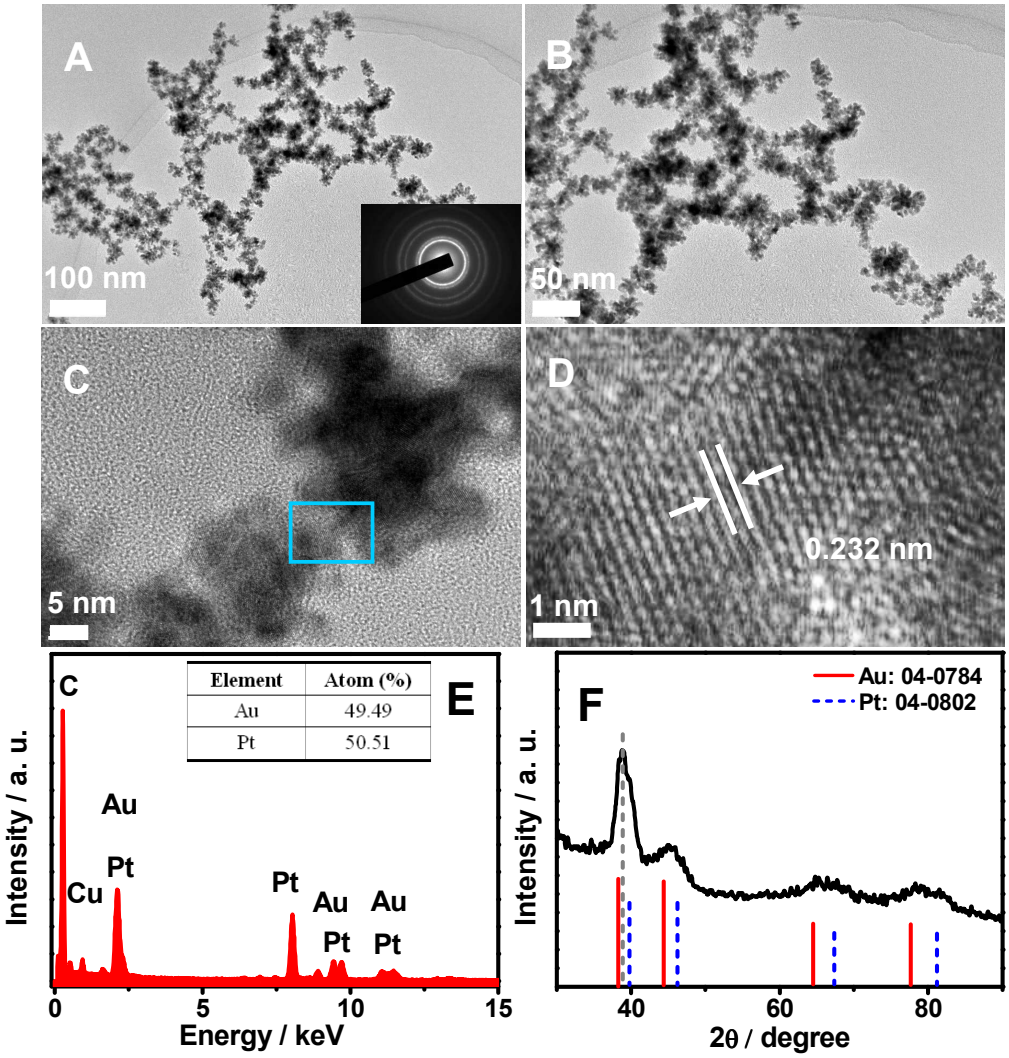

Journal of Materials Chemistry A Accepted Manuscript

Fig. 2

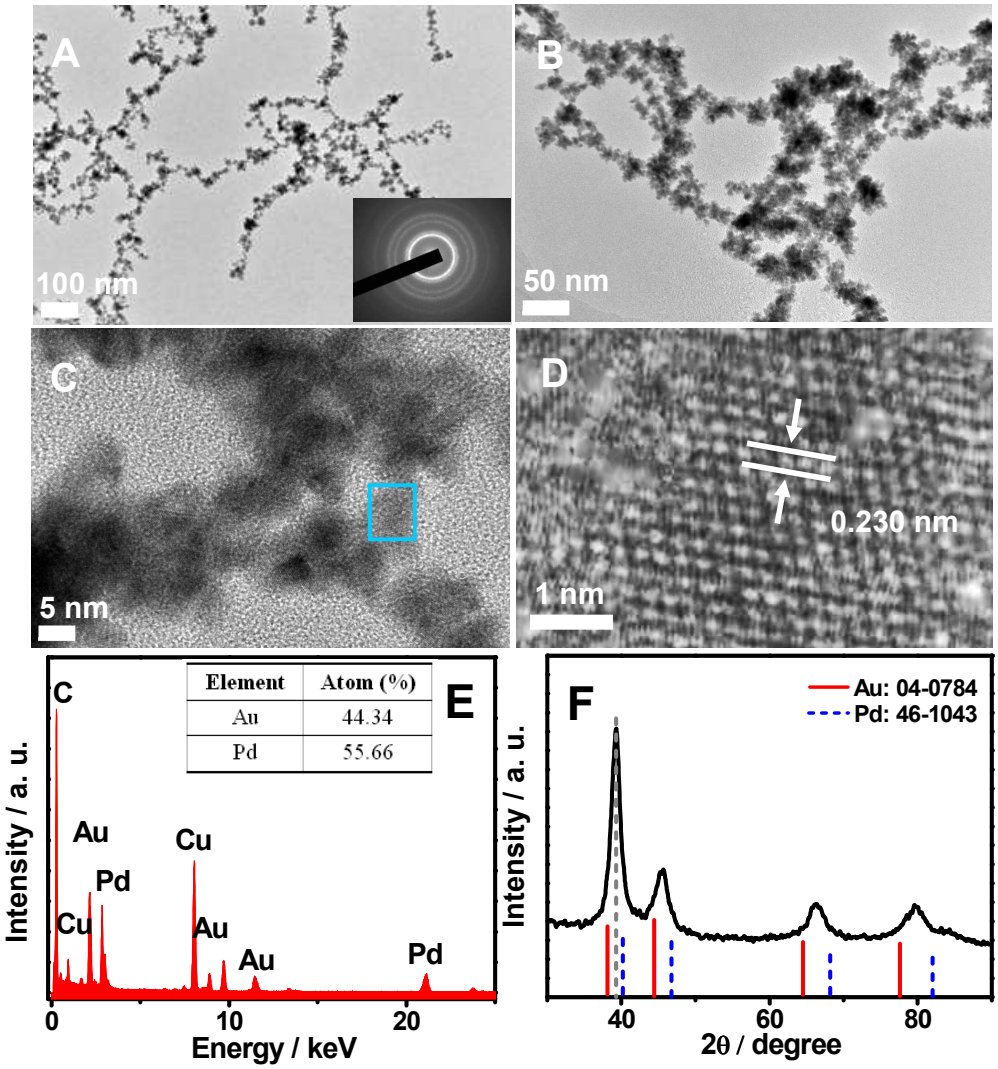

Journal of Materials Chemistry A Accepted Manuscript

Fig. 3

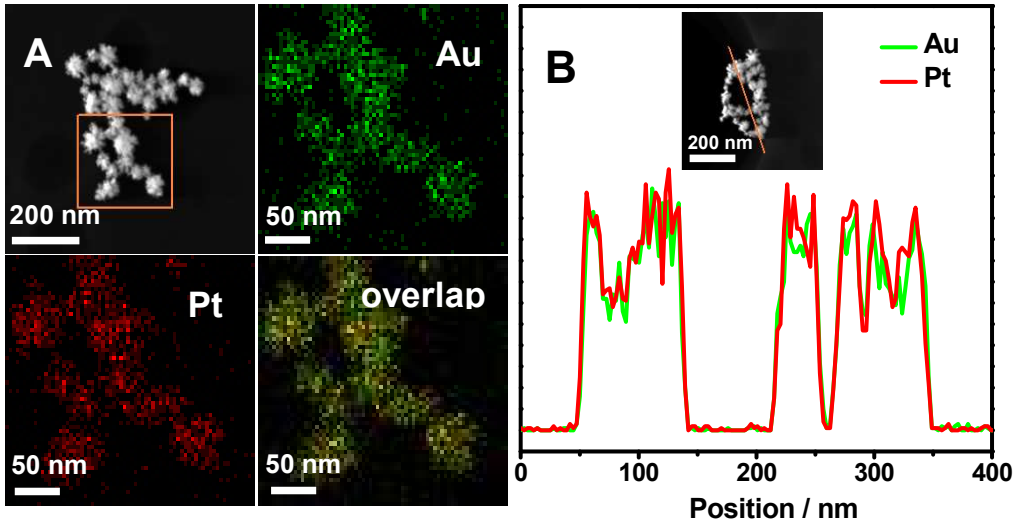

Journal of Materials Chemistry A Accepted Manuscript

Fig. 4

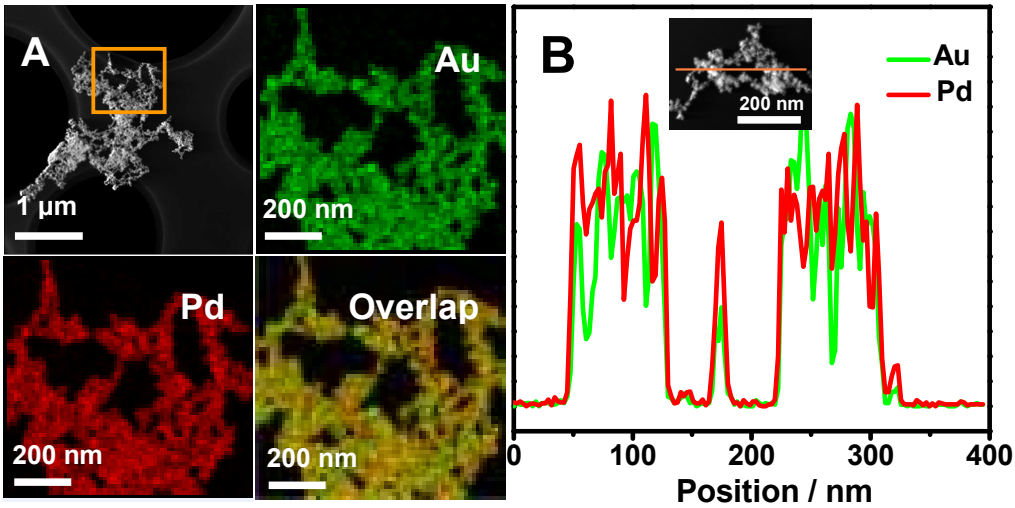

Journal of Materials Chemistry A Accepted Manuscript

Fig. 5

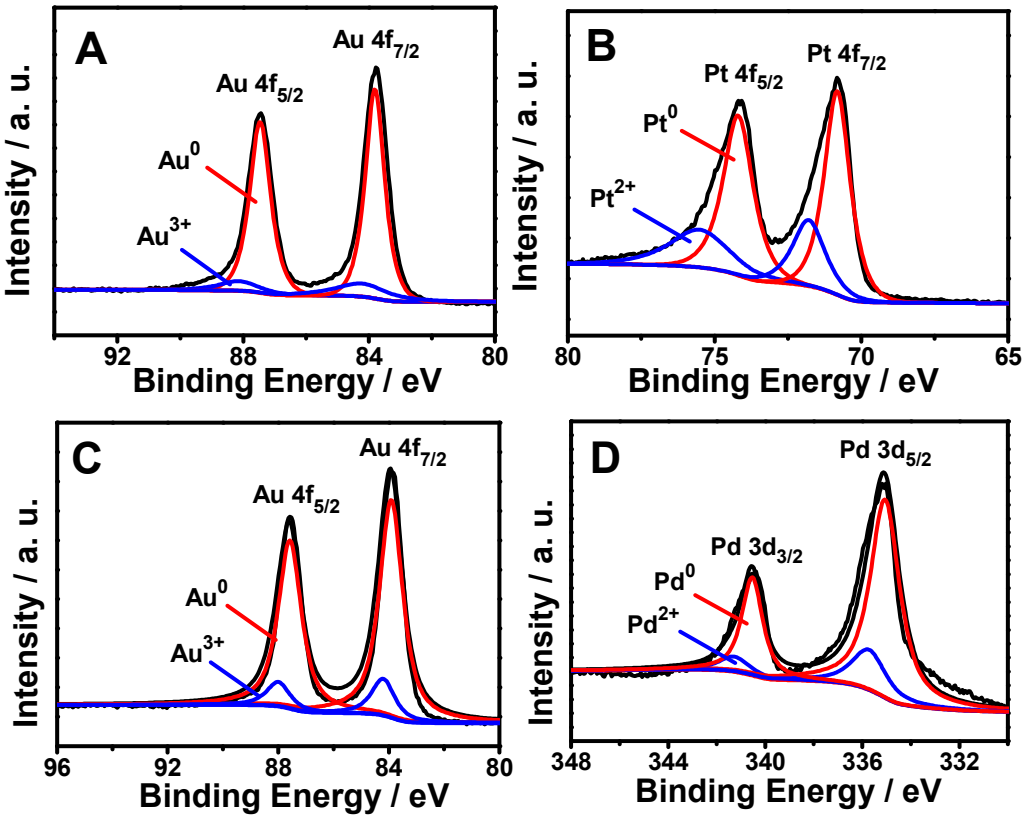

Journal of Materials Chemistry A Accepted Manuscript

Fig. 6

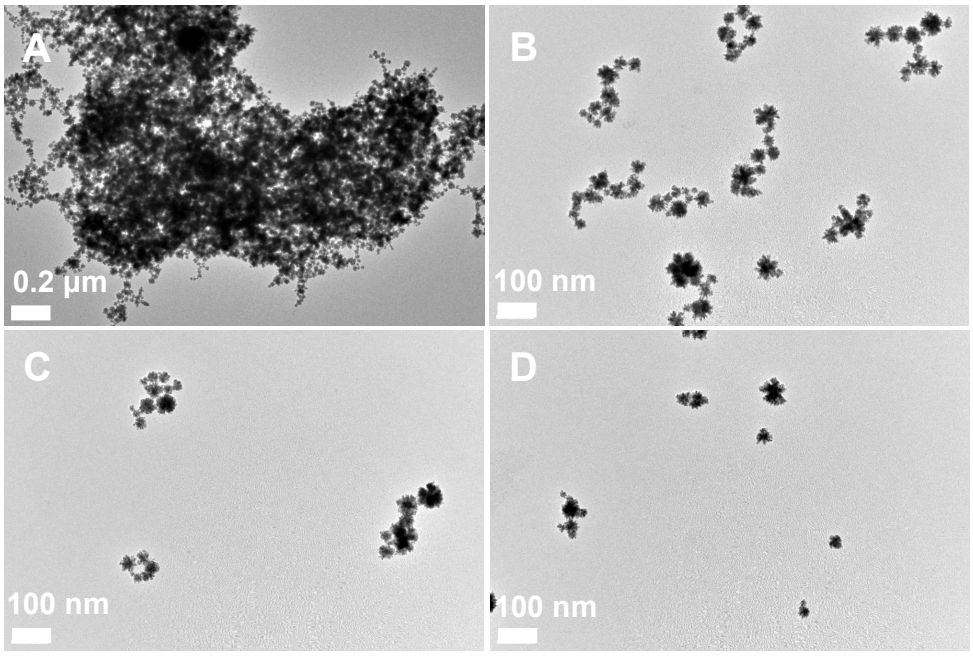

Journal of Materials Chemistry A Accepted Manuscript

Fig. 7

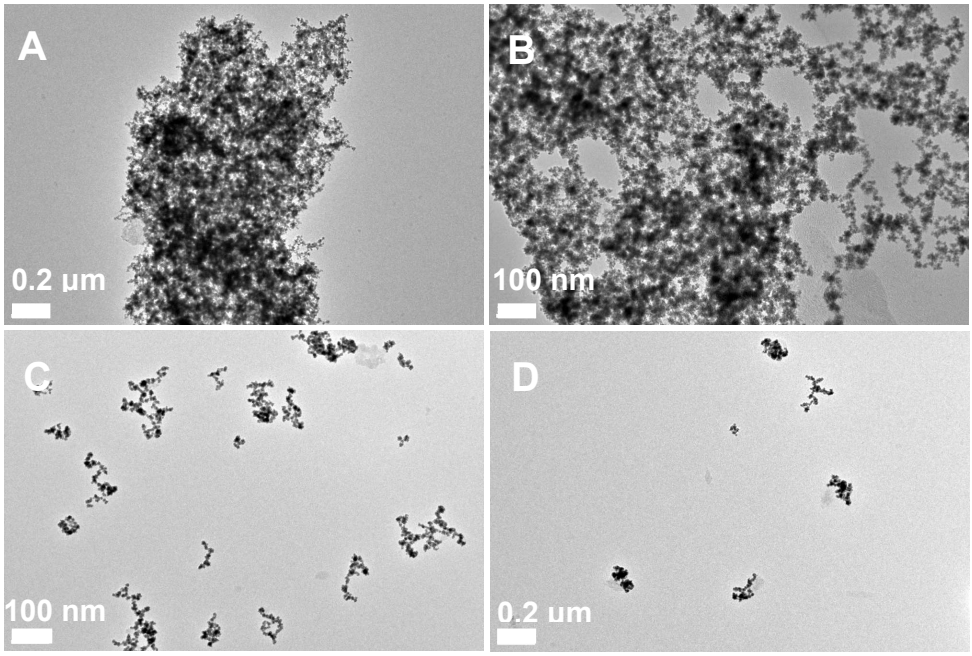

Journal of Materials Chemistry A Accepted Manuscript

Fig. 8

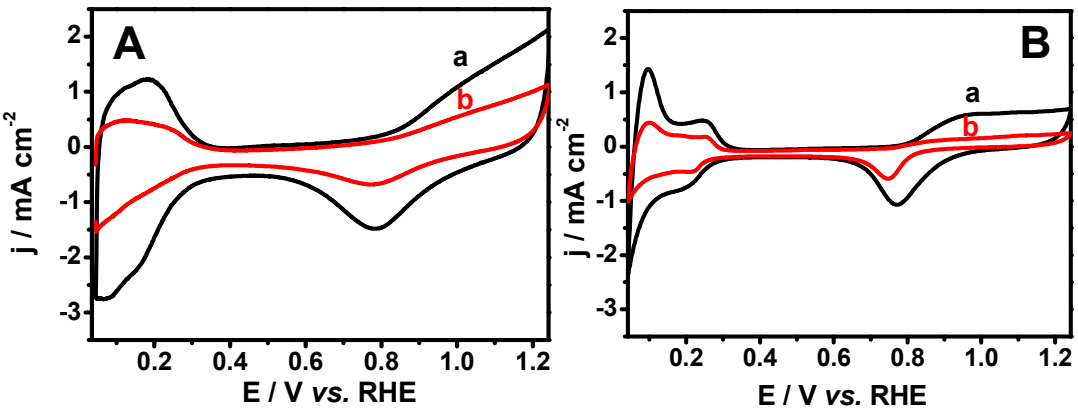

Journal of Materials Chemistry A Accepted Manuscript

Fig. 9

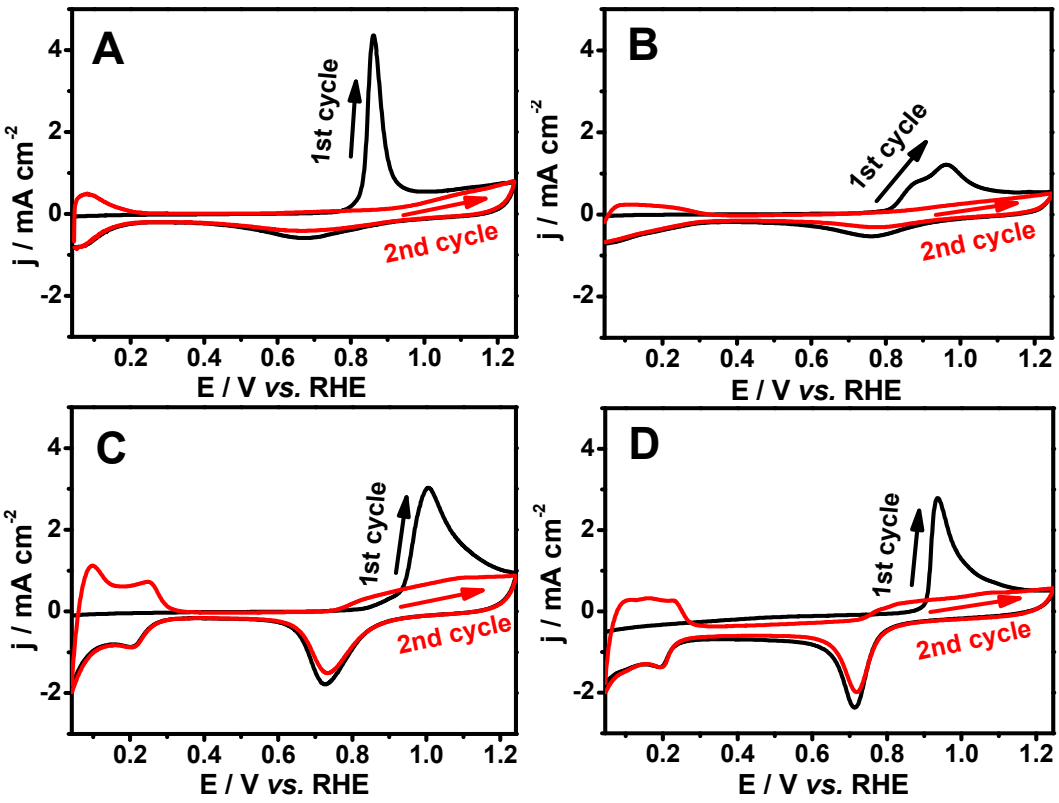

Journal of Materials Chemistry A Accepted Manuscript

Fig. 10

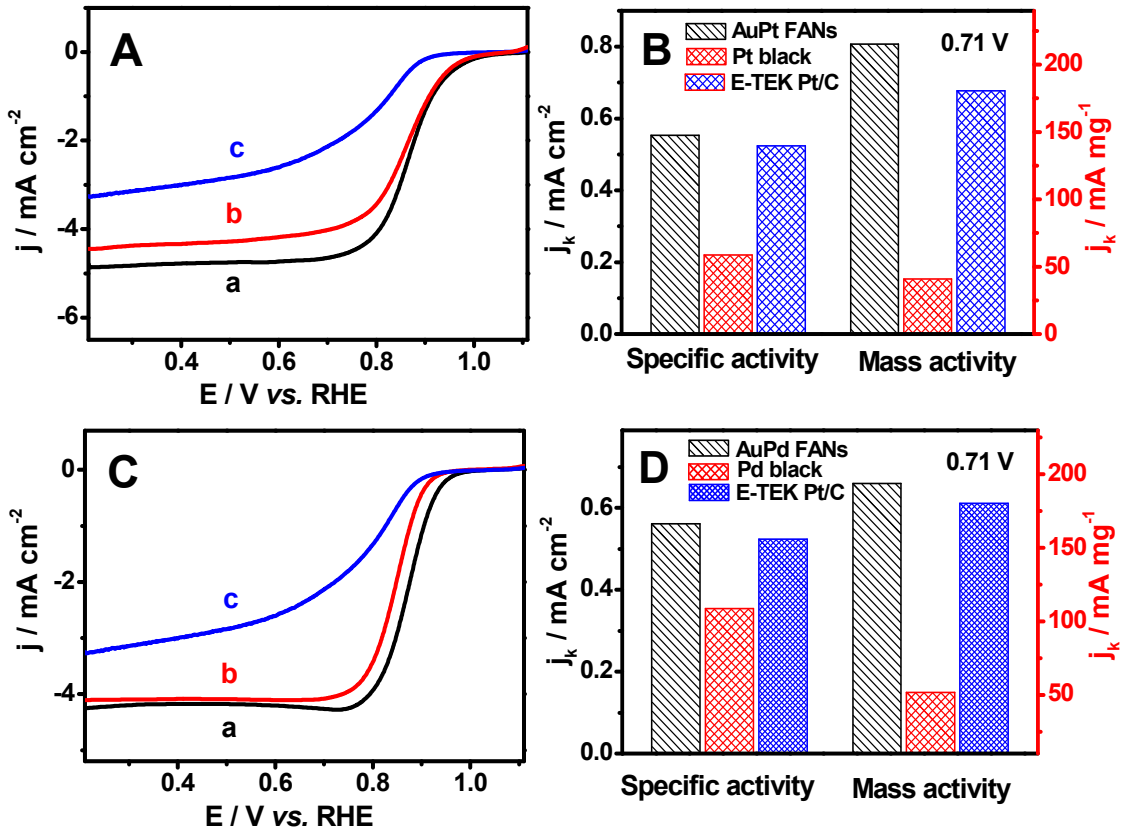

Journal of Materials Chemistry A Accepted Manuscript

Fig. 11

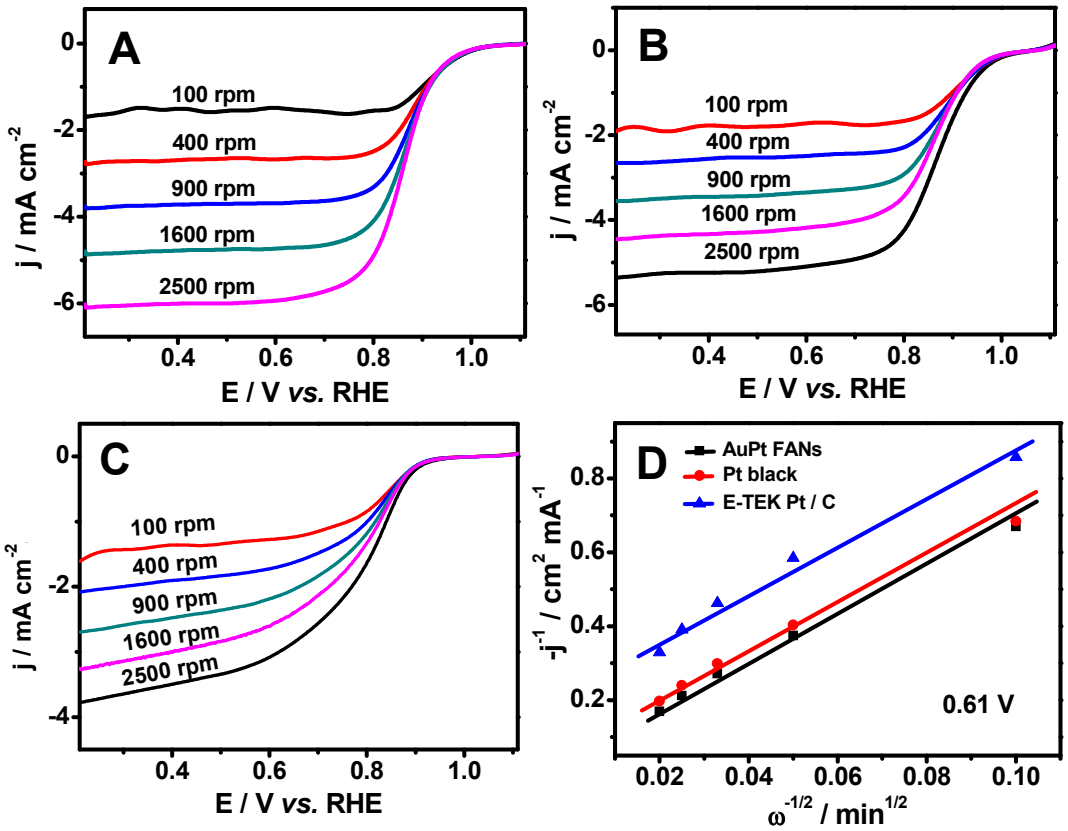

Journal of Materials Chemistry A Accepted Manuscript

Fig. 12

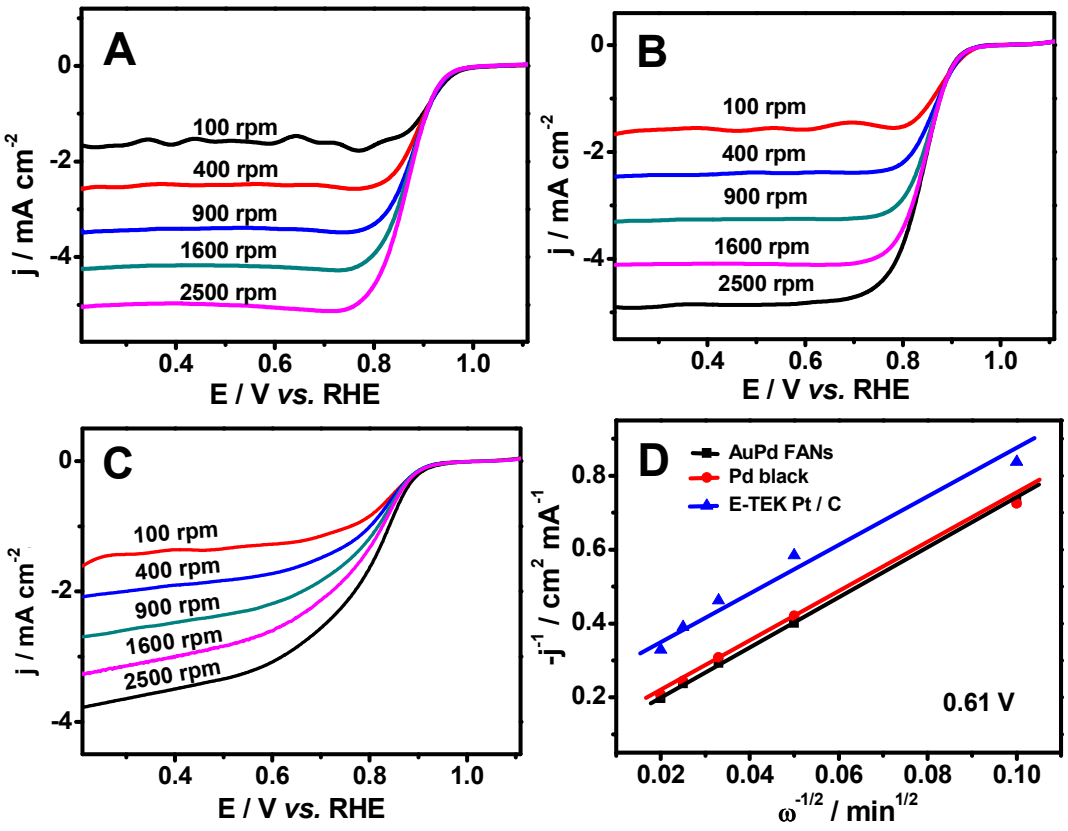

Journal of Materials Chemistry A Accepted Manuscript

Fig. 13

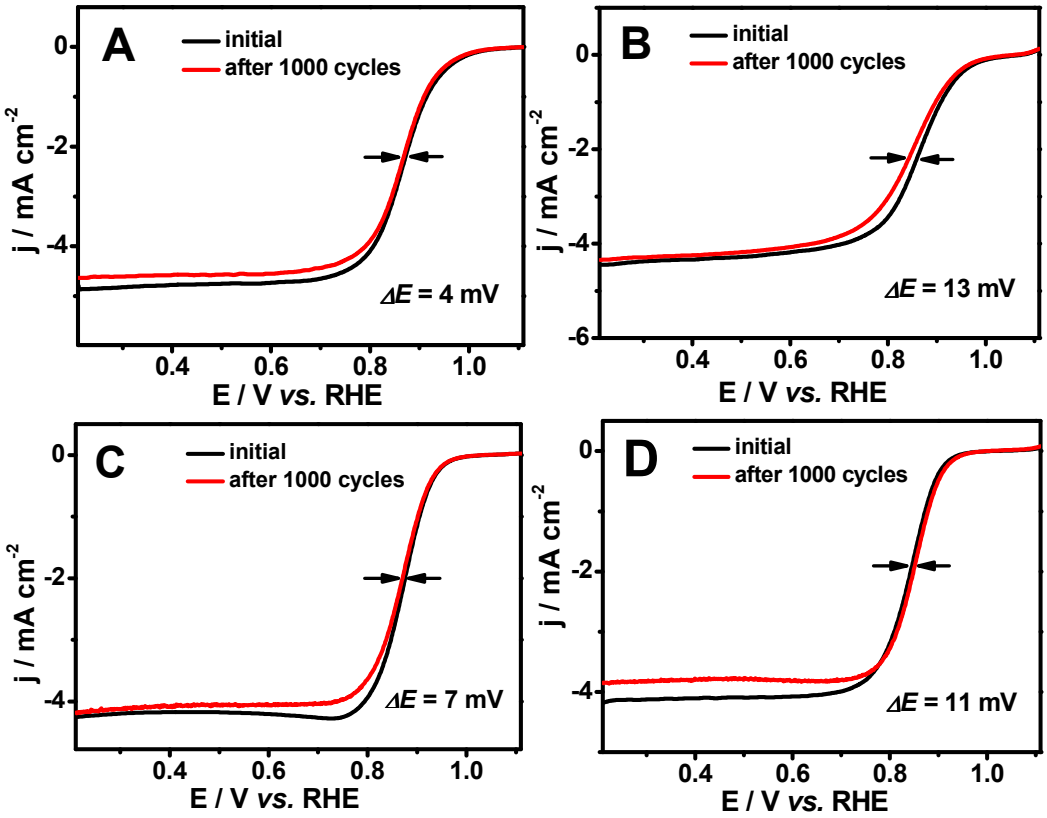

Journal of Materials Chemistry A Accepted Manuscript

Graphical Abstract

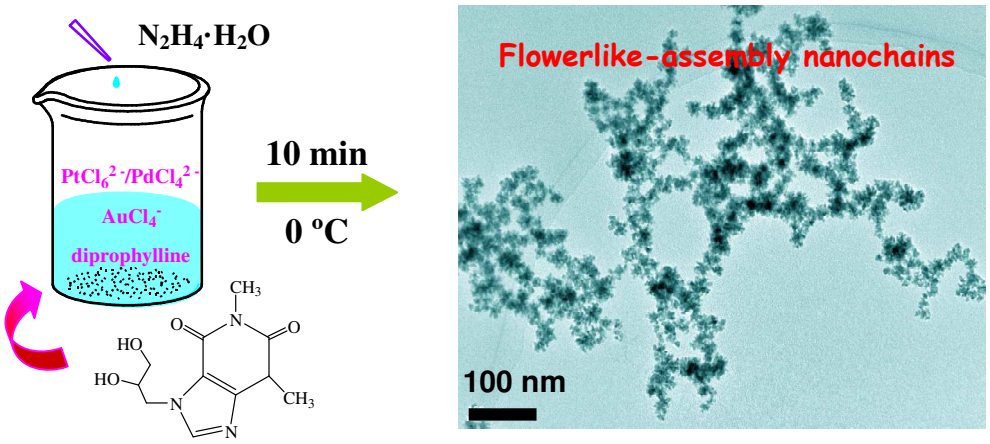

A facile general strategy was designed for preparation of AuM (M = Pt or Pd) alloyed flowerlike-assembly nanochains (FANs), with the assistance of diprophylline as a structure directing agent and a stabilizing agent. The as-prepared nanochains exhibited improved electrocatalytic performance for ORR.

Journal of Materials Chemistry A Accepted Manuscript